Available online at www.sciencedirect.com
ScienceDirect
Energy Conversion and Management 49 (2008) 54–61
ENERGY CONVERSION & MANAGEMENT
www.elsevier.com/locate/enconman

Numerical simulation of supercritical CO_2 injection into subsurface rock masses

Kenta Sasaki [a,*], Takashi Fujii [a], Yuichi Niibori [b], Takatoshi Ito [c], Toshiyuki Hashida [a]

[a] *Fracture and Reliability Research Institute, Tohoku University, Sendai 980-8579, Japan*
[b] *Department of Quantum Science and Energy Engineering, Graduate School of Engineering, Tohoku University, Sendai 980-8579, Japan*
[c] *Institute of Fluid Science, Tohoku University, Sendai 980-8577, Japan*

Received 12 October 2006; accepted 20 May 2007
Available online 23 July 2007

Abstract

Carbon dioxide (CO_2) is considered to be one of the greenhouse gases that may contribute most to global warming on the earth. Disposal of CO_2 from stationary sources into subsurface structures has been suggested as a possible means for reducing CO_2 emissions into the atmosphere. However, much remains to be done in the issues regarding the safety and reliability of CO_2 geological sequestration. In this study, we have developed a simulation code by using the mathematical model of two phase flow in porous media to analyze the flow dynamics in the subsurface. The equation of state for CO_2 covering the fluid region from the triple point to the supercritical region is employed to model the states of CO_2 gas, liquid and supercritical state. The correct understanding of the CO_2 state under the geological formation condition is an important factor to predict the injection pressure and CO_2 fluid permeation because the fluid density has a great effect on the injection behavior. The numerical simulation was implemented under several geological conditions including gas, liquid and supercritical states to examine the optimal injection condition. Comparing the numerical results obtained using the equation of state for CO_2 with those obtained using the ideal gas equation, it has been shown that the difference in the injection pressure appears to be significant near the condition of the critical point of CO_2 and the phase equilibrium curves between the gas and liquid states. The numerical simulation has been implemented to examine the effect of the reservoir condition on the injection behavior. The injection pressure is decreased at the lower reservoir temperature and higher hydrostatic pressure condition. The CO_2 permeation is also strongly affected by the reservoir condition, and the spatial CO_2 saturation becomes higher with increasing reservoir temperature. It has been demonstrated that the simulation code developed in this study may be useful to provide knowledge required to select the reservoir condition for CO_2 geological sequestration.

PACS: 91.65.My

Keywords: CO_2 geological sequestration; Numerical simulation; Supercritical CO_2; Two phase flow

1. Introduction

Human activity since the industrial revolution has had the effect of increasing the concentration of atmospheric greenhouse gases such as carbon dioxide (CO_2) [1]. Increasing concentrations of greenhouse gases lead to enhancing the greenhouse effect. A reduction in the release rate of CO_2 to the atmosphere is considered as essential for control of global warming. One way of achieving CO_2 reduction is to dispose of CO_2 in deep aquifers [2]. Deep aquifers have a large potential for CO_2 sequestration in geological media in terms of volume and duration. The conceptual model of CO_2 geological sequestration is shown in Fig. 1. CO_2 can be stored in aquifers in three ways. First, CO_2 can be hydrodynamically trapped as a gas or supercritical fluid in deep aquifers. Because of a very long flow

* Corresponding author. Tel.: +81 22 795 7524; fax: +81 22 795 4311.
E-mail address: ksasaki@rift.mech.tohoku.ac.jp (K. Sasaki).

0196-8904/$ - see front matter © 2007 Elsevier Ltd. All rights reserved.
doi:10.1016/j.enconman.2007.05.015

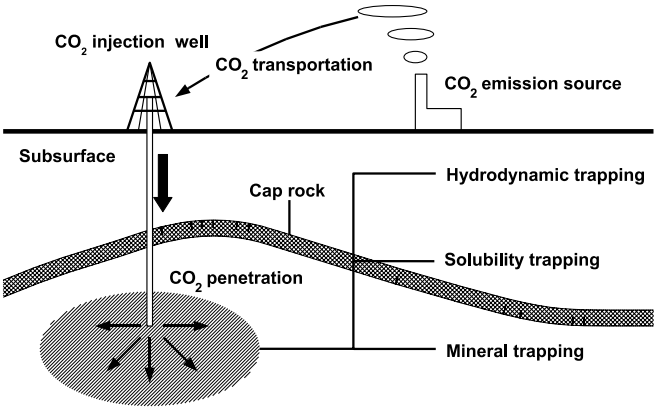

Fig. 1. Schematic illustration of CO_2 sequestration.

path, it would take a long time for the CO_2 to reach the surface. This process is called hydrodynamic trapping [3,4]. It may be the controlling mechanism for the initial period of CO_2 storage. Second, CO_2 can dissolve in the groundwater. It is considered that CO_2 dissolution in the water may increase the capacity of the reservoir to sequester CO_2 because of decreasing the volume of injected CO_2. The solubility of CO_2 in groundwater depends on the reservoir pressure, temperature and salinity. This process is referred to as solubility trapping [5]. It may be an important mechanism at the period of injection because the pressure increase caused by CO_2 injection enhances CO_2 dissolution into the formation water. Third, the chemistry between formation water and rock mineralogy plays an important role in determining the potential for CO_2 capture through geochemical reactions. The dissolved CO_2 in water can react with minerals in the geologic formation, leading to the precipitation of secondary carbonates. This process is called mineral trapping [3,6]. CO_2 can be permanently sequestered in deep aquifers because mineral trapping would lead to CO_2 immobilization. The fluid in the aquifer consists of groundwater and gas or supercritical CO_2. The multi-phase system in the aquifer is formed by CO_2 injection, and one phase affects the flow behavior of the other phase [7].

While CO_2 sequestration into deep aquifers is an attractive way to reduce the concentration of atmospheric CO_2, much remains to be done in the issues regarding the flow dynamics and the mechanical response in the reservoir such as the leakage of CO_2 from the aquifer and excessive pressurization of the injection well [8]. It is crucially important to understand the fluid flow and pressure response in the reservoir in order to ensure the reliability of CO_2 injection into the subsurface. Some simulation studies dealing with CO_2 disposal into aquifers have been performed with existing reservoir simulators. Some numerical simulations have been implemented by using TOUGH2 [9], which is a general purpose multiphase flow simulator, or TOUGH2 with some modules for adapting to CO_2 geological sequestration to evaluate the capability of this technology [10]. Numerical simulation by using TOUGHREACT involves not only multiphase flow but also chemical interactions between the reservoir fluids and the rock [3]. However, the treatment of the fluid density for the computation of fluid flow is insufficient. Particularly, there are few numerical investigations with involvement of the consideration of all the CO_2 fluid states, namely, gas, liquid and supercritical states.

Thus, we have developed a simulation code by using the mathematical model of two phase flow in porous media. The simulation code developed in this study takes into account the state for CO_2 covering the triple point temperature and pressure to the supercritical region [11]. Our treatment includes a realistic representation of the CO_2 density of the gas, liquid and supercritical states. The CO_2 density changes drastically near the liquid-gas phase equilibrium condition or the critical point of CO_2, and the density change affects the injection behavior. Large scale CO_2 injections have been performed at several field sites, including Alberta, Canada [12,13], Sleipner North Sea [14,15], Gippsland Basin, Australia [16,17] and Nagaoka, Japan [18]. The temperature and pressure conditions of CO_2 expected for those field sites are plotted on the phase diagram of CO_2 as shown in Fig. 2. As exemplified in Fig. 2, the CO_2 temperature and pressure conditions fall in the supercritical region. The data of Fig. 2 may indicate the importance of incorporating the phase change of CO_2 in the analysis of CO_2 injection. The paper presented here focuses on issues of the site dependence of the injection behavior. The geothermal and hydrostatic pressure gradients for the vertical direction of the calculation region are employed to take into account realistic reservoir conditions for CO_2 geological sequestration. Simulation results are presented in order to examine the impact of CO_2 injection for various reservoir temperature and pressure conditions. Finally, we investigate the effective injection condition for CO_2 sequestration into the aquifer.

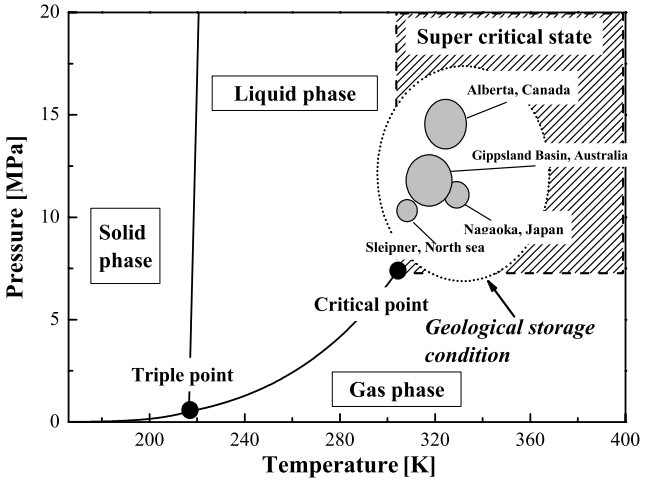

Fig. 2. Phase diagram of CO_2 covering the solid region to supercritical state.

2. Mathematical model and computation conditions

To develop a simulation code of CO_2 injection, the model of two phase flow in porous media was employed. The two phases are assumed to be groundwater as wetting phase and CO_2 fluid as non-wetting phase. The equation of state for CO_2 used in this study can calculate the CO_2 density covering the fluid region from the triple point condition to the supercritical region. The CO_2 density was calculated by two ways; one is the equation of state for CO_2 and another is the ideal gas equation. The formulation of the numerical model and theoretic explanation is as follows.

2.1. General form of two phase flow

The mass balance equation for two phase flow in a porous medium for each phase α (wetting or non-wetting) is given by (for example [7,19])

$$\frac{\partial(mS_\alpha\rho_\alpha)}{\partial t} + \mathrm{div}(\rho_\alpha \mathbf{v}_\alpha) = 0. \tag{1}$$

where the subscript α refers to w for the water phase and n for the CO_2 phase, m is the porosity, S_α the saturation, ρ_α the density, t time and $\mathbf{v}_\alpha$ the Darcy flux velocity. Darcy's law extended to two phase flow can be written for each phase as

$$\mathbf{v}_\alpha = -\frac{k_{r\alpha}}{\mu_\alpha}\mathbf{K}(\mathrm{grad}\, p_\alpha - \rho_\alpha \mathbf{g}), \tag{2}$$

where $\mathbf{K}$ is the absolute permeability, $k_{r\alpha}$ the relative permeability, μ_α the viscosity, p_α the pressure and $\mathbf{g}$ the acceleration due to gravity. Inserting Eq. (2) into Eq. (1) yields the general form of the two phase flow differential equation, as follows:

$$\frac{\partial(mS_\alpha\rho_\alpha)}{\partial t} - \mathrm{div}\left\{\rho_\alpha \frac{k_{r\alpha}}{\mu_\alpha}\mathbf{K}(\mathrm{grad}\, p_\alpha - \rho_\alpha \mathbf{g})\right\} = 0. \tag{3}$$

The multiphase system in porous media is characterized by parameters such as the capillary pressure, relative permeability and saturation relationship. Relative permeability is a ratio of the effective permeability of a particular fluid at a particular saturation to the absolute permeability of that fluid at total saturation. Capillary pressure is defined as the pressure difference across the interface between two immiscible fluids. These relationships were considered by using the van Genuchten model [19,20]. According to the van Genuchten model, the relationships between the relative permeabilities and the effective saturation are given by

$$k_{rw} = S_e^{\epsilon}\{1 - (1 - S_e^{1/\psi})^{\psi}\}, \tag{4}$$

$$k_{rn} = (1 - S_e)^{\gamma}(1 - S_e^{1/\psi})^{2\psi}, \tag{5}$$

where S_e is the effective saturation, ϵ, γ and ψ are parameters that are determined by the shape of the pores. The effective saturation is described as follows:

$$S_e = \frac{S_w - S_{wr}}{1 - S_{wr} - S_{nr}} = \{1 + (\eta p_c)^{l}\}^{-\psi}, \tag{6}$$

where $S_{\alpha r}$ is the residual saturation, p_c the capillary pressure and η, $l(=1 - 2/\psi)$ are rock specific parameters determined by the connectivity and shape of the pores. The capillary pressure, however, was neglected under the assumption that the injection pressure would be much higher than the capillary pressure ($p_w = p_n$). Fig. 3 shows the relative permeability curves as a function of effective saturation, which was used in this study. According to the literature [19], typical values for the parameters ϵ, γ and ψ are 1/2, 1/3 and 0.77, respectively. These representative values were used for ϵ, γ and ψ throughout the numerical simulation of this study.

2.2. Equation of state for CO_2

For computation of the CO_2 density for reservoir pressure and temperature, we employed the equation of state developed by Span and Wagner [11]. The equation of state is built by applying a fitting procedure for reliable experimental data and an optimized mathematical form. The details of the fitting and optimization method ares written in the literature [21]. The fundamental equation is expressed in a form of the Helmholtz energy A with the two independent variables density ρ and temperature T. The dimensionless Helmholtz energy $\phi = A/(RT)$ is commonly split into a part depending on the ideal gas behavior ϕ^0 and a part that takes into account the residual fluid behavior ϕ^r, namely

$$\phi(\delta, \tau) = \phi^0(\delta, \tau) + \phi^r(\delta, \tau), \tag{7}$$

where $\delta = \rho/\rho_c$ is reduced density and $\tau = T_c/T$ is the inverse reduced temperature. Both the density ρ and the temperature T are reduced with their critical values, ρ_c and T_c with $\rho_c = 467.6\ \mathrm{kg/m^3}$ and $T_c = 304.1282\ \mathrm{K}$, respectively. Since the Helmholtz energy is one form of a fundamental equation as a function of density and temperature, all the

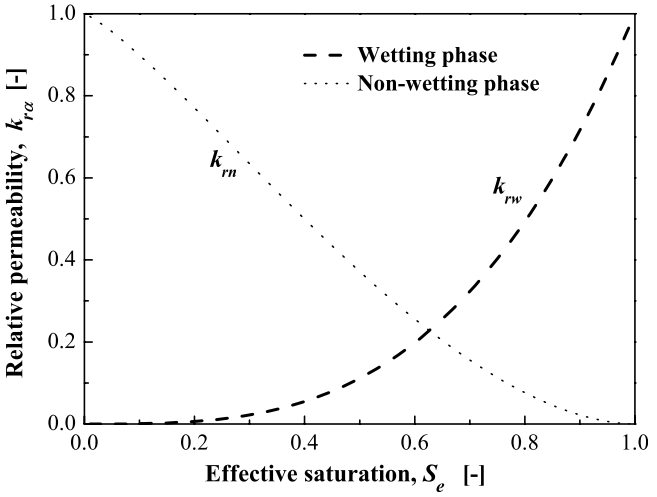

Fig. 3. Relative permeability vs. effective saturation curves for each phase.

thermodynamic properties of CO_2 can be obtained by combining derivatives of Eq. (7). The pressure for the density and temperature is given by

$$\frac{p(\delta,\tau)}{\rho RT} = 1 + \delta\phi^{\mathrm{r}}_{\delta}, \tag{8}$$

where $\phi^{\mathrm{r}}_{\delta} = (\partial\phi^{\mathrm{r}}/\partial\delta)_{\tau}$. On the basis of Eq. (8), the CO_2 density can be calculated from the pressure and temperature with the thermodynamic definition. The CO_2 density calculated by using the equation of state for CO_2 is shown in Fig. 4 together with the phase equilibrium curve between the liquid and gas states. The CO_2 density changes drastically under conditions near the critical point and the phase equilibrium curve.

2.3. Numerical method and boundary conditions

For the spatial discretization of Eq. (3), we implemented a finite differential method. Since the system of equations has strong nonlinear properties, we used the de-coupled method [19,22]. The idea of this method is to eliminate the saturation terms from the flow equations to obtain an equation that involves only one dependent variable. Assuming that the non-wetting phase is compressible and the wetting phase is incompressible, the chain rule is applied to Eq. (3), and the resulting equation that includes only pressure as a variable is given by

$$\begin{aligned}
&\nabla^2 p_{\mathrm{w}} = \xi\frac{\partial p_{\mathrm{w}}}{\partial t} + \xi\frac{\partial p_{\mathrm{c}}}{\partial t} - \zeta\{\nabla\rho_{\mathrm{w}}\nabla p_w\},\\
&\xi = \frac{m}{\mathbf{K}(\lambda_w+\lambda_n)}\frac{S_n}{\rho_n}\left(\frac{d\rho_{\mathrm{n}}}{dp_{\mathrm{n}}}\right),\\
&\zeta = \frac{\lambda_n}{\lambda_w+\lambda_n}\frac{1}{\rho_{\mathrm{n}}},
\end{aligned} \tag{9}$$

where λ_α is the mobility ($=k_{\mathrm{r}}\alpha/\mu_\alpha$).

The schematic illustration of the calculation region and boundary conditions is shown in Fig. 5. The numerical simulation was conducted for the horizontal (X)- vertical (Z) two dimensional model domain (200 m × 200 m) to take into account the hydrostatic pressure gradient (0.01 MPa/m) and the geothermal gradient (0.1 K/m). In addition, in order to evaluate the effects of reservoir conditions on injection behavior, the reservoir temperature and hydrostatic pressure at the upper boundary of the calculation region was varied from 273 K to 473 K and 5 to 25 MPa, respectively. The calculation region was divided into 40 grids in both the vertical and horizontal directions and equally spaced. The injection point was set at the center of the calculation region, and the saturation S_{n} was set to be 1.0 at the injection point to simulate CO_2 injection. The saturation in the calculation region, except for the injection point, was set to be 0.10 as an initial condition, which indicated that the reservoir was mainly filled with water before CO_2 injection was started. The flow rate at the injection point q_{n} was fixed at 5.0 kg/s for every simulation trial, and the flow rate was converted to vector components for each direction by using the following equation, which is derived from fluid dynamics definition [23]:

$$q_{\mathrm{n}} = \rho_{\mathrm{n}} B \mathbf{v}_{\mathrm{n}}, \tag{10}$$

where B ($=2\pi r\,L$) is the surface area of the borehole of the injection well, r ($=0.1m$) the radius of the injection well and L($=20m$) the length of the open hole. Staggered grids were used for discretization in order to increase the accuracy and stability of the numerical simulation [23]. The key feature here is that the pressures and velocities are calculated at different grid points. An advantage of the staggered grid is that when the velocity is calculated, a central difference for $\partial p_\alpha/\partial x$ is based on adjacent pressure points. Generally, these procedures enhance the accuracy of the numerical simulation and prevent pressure oscillation.

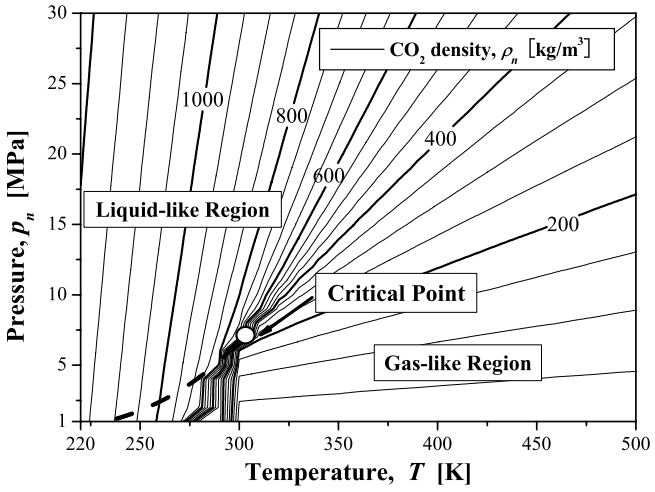

Fig. 4. Pressure-temperature diagram for CO_2 density calculated by the equation of state for CO_2.

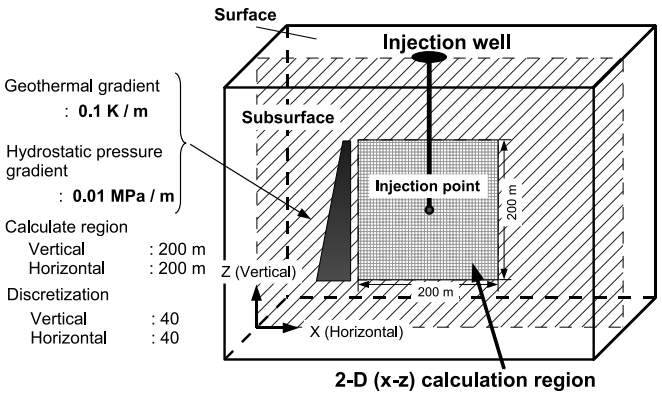

Fig. 5. Schematic illustration of 2-D calculation region. The geothermal and hydrostatic pressure was given linear profile for the analytic depth.

3. Results and discussion

We implemented numerical simulations under various temperature and hydrostatic pressure conditions. The hydrostatic pressure covered in this study was 5–25 MPa, and the temperature was in the range of 273–473 K. The

relevant parameters used for the simulation such as reservoir rock and fluid properties are shown in Table 1. The calculation region was assumed to be homogeneous, and the reservoir permeability and porosity was kept constant. For comparison, two numerical simulations were conducted under identical temperature and pressure conditions. One simulation was conducted using CO_2 density calculated from the ideal gas equation, and the other calculation was executed based on the equation of state for CO_2 described in the preceding section.

Here, injection pressure p_{inj} is defined as the differential pressure at the injection point, namely,

$$p_{inj} = p_{n,inj} - p_{hyd,inj}, \tag{11}$$

where $p_{hyd,inj}$ is the initial hydrostatic pressure (reservoir pore pressure), which depends on the depth of the injection point and $p_{n,inj}$ is the CO_2 pressure at the injection point. Fig. 6 shows the numerical result of injection pressure vs. time for different temperatures, obtained with the equation of state for CO_2. The temperature shown is the rock mass temperature. The higher is the reservoir temperature, the larger is the injection pressure. This is because the CO_2 density tends to decrease with increasing temperature. As shown in Fig. 6, the injection pressure increases very rapidly at the initial stage and then tends to saturate at longer injection times. The approximate time when the pressure saturates is indicated by an arrow for each curve. A higher temperature requires a longer period of injection due to the decrease in CO_2 density. With the injection flow rate of 5.0 kg/s, which is used for Nagaoka field [18], the injection pressure appears to reach a saturation pressure within 1 day. The saturated pressure computed by the numerical simulation is plotted in Fig. 7 on the hydrostatic pressure and temperature diagram. In the case of the result using the equation of state for CO_2, the contour of injection pressure is narrow when the hydrostatic pressure is relatively

Table 1
List of the relevant parameters used

Reservoir rock			
Permeability	**K**	1.0×10^{-13}	[m^2]
Porosity	m	0.20	[–]
Temperature (injection point)	T	273–473	[K]
Pressure (injection point)	p_{hyd}	5.0–25.0	[MPa]
Fluid			
Water (wetting phase)			
Density	ρ_w	1000	[kg/m^3]
Viscosity	μ_w	0.283×10^{-3}	[kg/(ms)]
Residual saturation	S_{wr}	0.05	[–]
CO_2 (non-wetting phase)			
Density	ρ_n	Calculated by eq. of state for CO_2	[kg/m^3]
Viscosity	μ_n	0.216×10^{-4}	[kg/(ms)]
Residual saturation	S_{nr}	0.05	[–]
Flow rate	q_n	5.0	[kg/s]

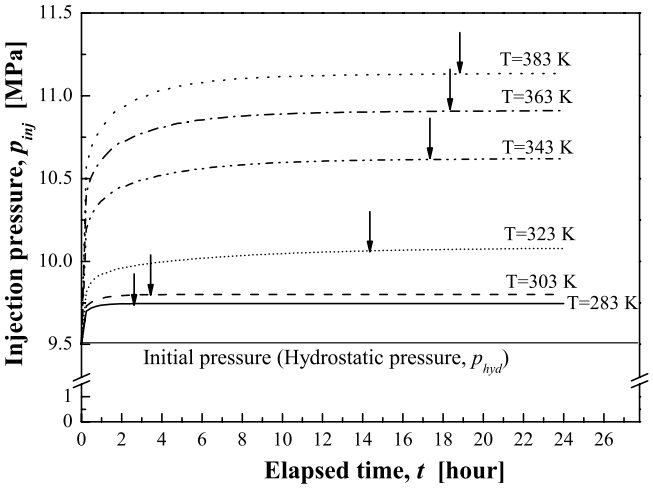

Fig. 6. Injection pressure vs. elapsed time curves for different reservoir temperature.

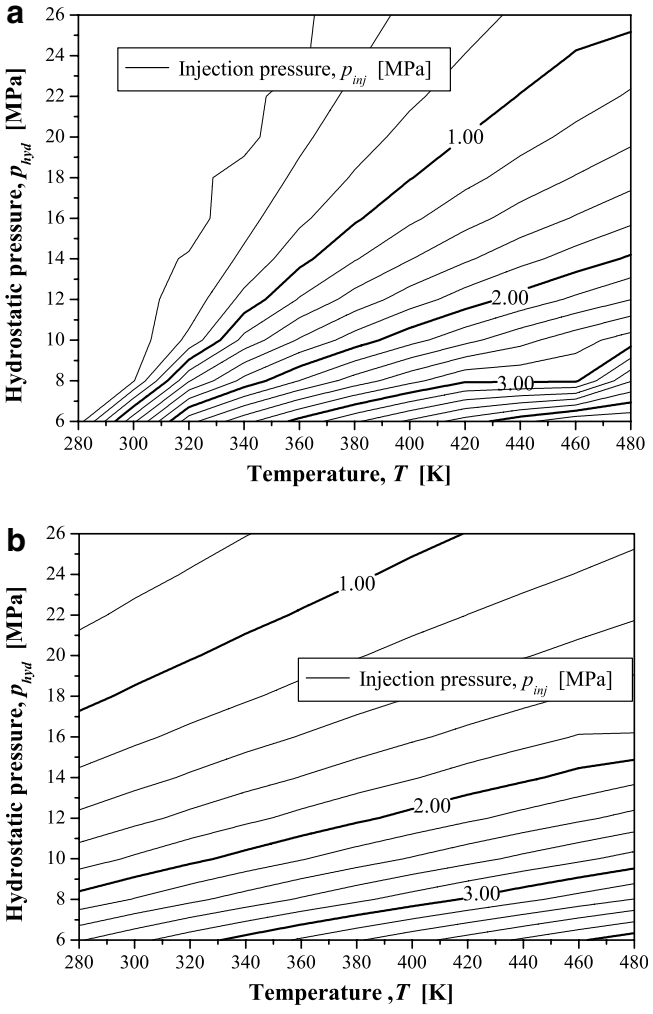

Fig. 7. Injection pressure diagram for each hydrostatic pressure and temperature. (a) CO_2 density is calculated by using equation of state for CO_2. (b) Fluid density is calculated by using ideal gas equation.

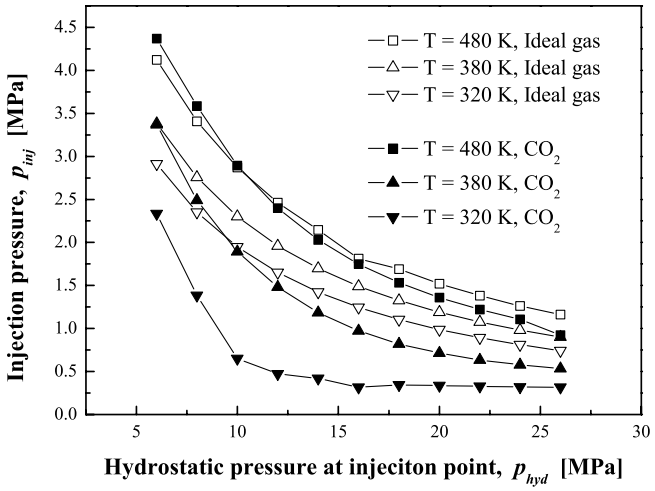

Fig. 8. Hydrostatic pressure versus injection pressure curves for different temperture. The solid lines with open symbol represent the results calculated by using ideal gas equation and the ones with closed symbol are calculated by the equation of state for CO_2.

lower. This result indicates that the injection pressure is sensitive to the slight change of reservoir pressure under the above mentioned condition. In addition, the reservoir condition close to the critical point of CO_2 yields a significant difference for the injection behavior between an ideal gas and CO_2. As seen in Fig. 8, the ideal gas equation tends to provide a good estimate of injection pressure at higher temperature conditions. Specifically, the ideal gas equation is sufficiently accurate when the temperature exceeds 380 K. When the ideal gas equation predicts higher injection pressure than that obtained with the equation of state for CO_2, the difference between the two predictions becomes significantly large when the condition of CO_2 is close to the critical point. It is clear that under the pressure and temperature conditions of the field scale CO_2 injections shown in Fig. 2, the ideal gas modeling of CO_2 is inaccurate to simulate actual CO_2 injection behavior. The comparison may demonstrate the use of the equation of state for CO_2 is necessary for prediction of the CO_2 injection behavior.

It is important to understand the time variation of the spatial saturation distribution caused by the CO_2 injection in order to evaluate the capacity and reliability for CO_2 storage. The spatial distributions of CO_2 saturation are shown in Fig. 9 for the CO_2 injection duration of 0.01, 0.10, 0.50 and 1 day. The temperature and hydrostatic pressure are 353 K and 8 MPa, respectively. The initial CO_2 saturation S_n is set to be 0.1 at every point.

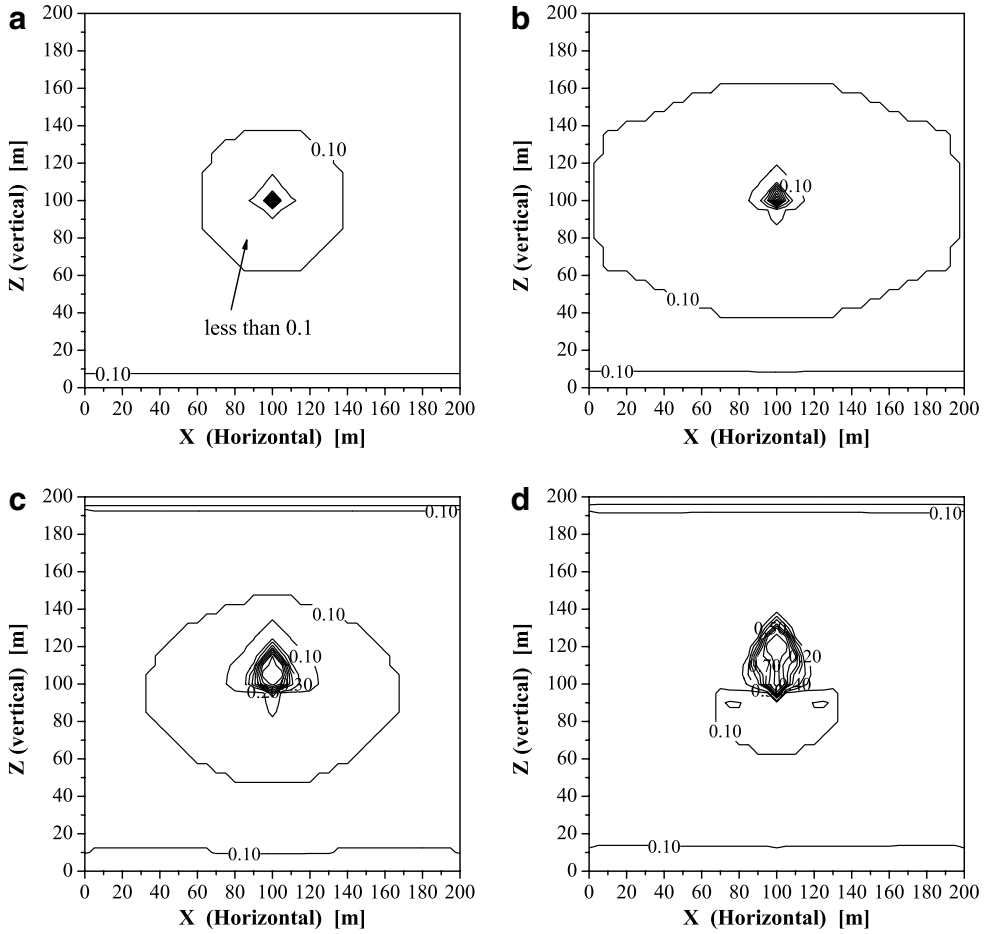

Fig. 9. CO_2 saturation distribution after CO_2 injection of 1 day. (a) t = 0.01 day; (b) t = 0.10 day; (c) t = 0.50 day; (d) t = 1.00 day.

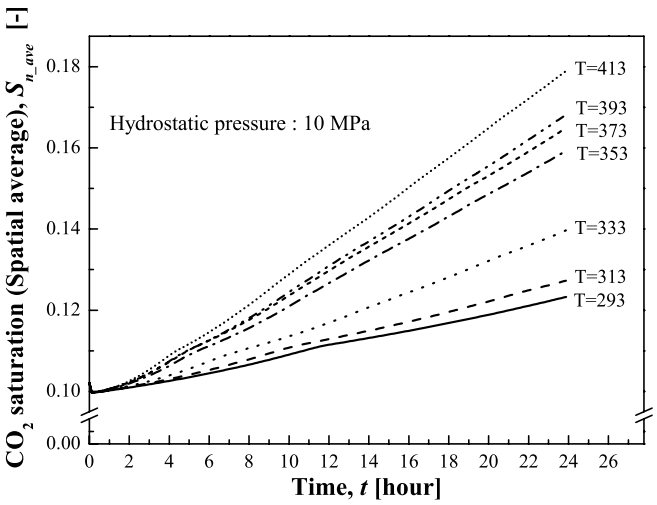

Fig. 10. The variation of spatial average of CO_2 saturation with time.

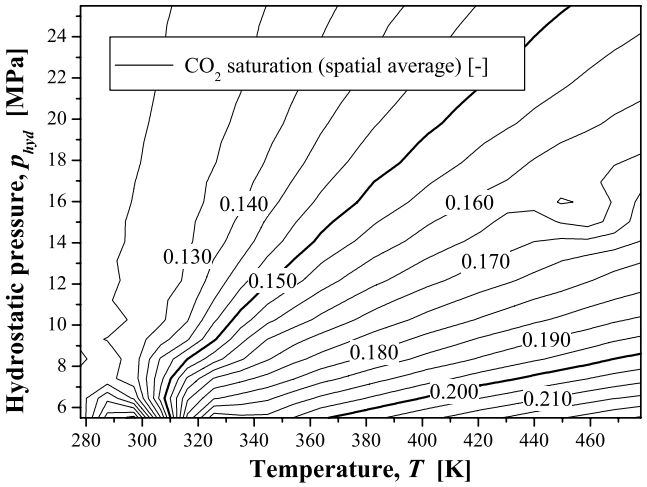

Fig. 11. The spatial average of CO_2 saturation distribution for different temperatures and hydrostatic pressures.

Initially, the injected CO_2 is observed to permeate in an isotropic fashion into the rock mass from the injection point, and the CO_2 region has an approximately circular shape. It is seen that there is a region around the injection point where the CO_2 saturation is slightly decreased. The lower region with the decreased CO_2 saturation may be due to compression of the CO_2 phase caused by CO_2 pressurization. As the injection progresses, the injected CO_2 permeates into the upper region, and no migration of CO_2 in the downward orientation is observed. The predominantly upward growth of the CO_2 region may be due to the effects of buoyancy and vertical pressure gradient in the hydrostatic pressure. Similar upward growth of the CO_2 region was also observed for all the other temperature and pressure conditions. The spatial average of CO_2 saturation is shown in Fig. 10 for temperatures from 293 to 413 K under a hydrostatic pressure of 10 MPa. A region selected to calculate the spatial average of the CO_2 saturation was $100\,m \times 100\,m$ whose central location comes from the injection point. It has been shown that the CO_2 region does not exceed the above calculation region within the CO_2 injection duration of 1 day. Initially, the CO_2 saturation decreases only slightly and increases monotonically almost in a linear fashion with respect to time. The initial slight decrease in CO_2 saturation may be caused by the compressed CO_2 volume surrounding the injection point, as already mentioned. It is seen from Fig. 10 that the CO_2 saturation becomes smaller when the temperature is lower. The result really indicates that the lower temperature condition requires a smaller rock volume for CO_2 storage compared to that of the higher temperature for the same hydrostatic pressure. The spatial average of CO_2 saturation after a CO_2 injection duration of 1 day is plotted in Fig. 11 for different hydrostatic pressures and temperatures. At the higher temperature regime, the averaged CO_2 saturation tends to become smaller when the hydrostatic pressure becomes higher. On the other hand, the averaged CO_2 saturation becomes less sensitive to the hydrostatic pressure for the lower temperature regime for hydrostatic pressures greater than approximately 10 MPa. Fig. 11 also indicates that there is a general trend that the lower is the temperature, the smaller is the averaged CO_2 saturation, suggesting smaller CO_2 reservoirs can be created by CO_2 injection at lower temperature compare to those at higher temperature. The temperature and pressure effects on the averaged CO_2 saturation are most likely caused by the variation of CO_2 density. The CO_2 density drastically changes under the temperature condition close to the critical point of CO_2. The numerical results obtained in this study point out that it is of importance to account for the equation of state for CO_2 for analyzing and evaluating CO_2 injections.

4. Conclusion

In this study, a two phase numerical model for simulation of CO_2 sequestration into underground structures is presented. To account for the proper CO_2 density for the gas, liquid and supercritical states, the equation of state for CO_2 is employed. The numerical simulation is implemented to investigate the feasibility of CO_2 injection behavior for reservoir hydrostatic pressure and temperature conditions because the controlling factor for CO_2 density is pressure and temperature. Modeling the injection and storage with the realistic representation of the CO_2 density into geological media has provided valuable insights into the injection behavior and has verified conformance with designing the CO_2 injection condition of the reservoir. The main results of the numerical simulation are described below.

The numerical simulations have been conducted to monitor the injection behavior with the treatment of the modeling with the realistic CO_2 density. Comparing the numerical results obtained using the equation of state for CO_2 with the results from modeling with the ideal gas

equation, the distinction in the injection pressure appears to be significant near the condition of the critical point of CO_2 and the phase equilibrium curves. Although modeling of the ideal gas equation for numerical simulation can be applied to predict the CO_2 injection behavior at high temperature and low hydrostatic pressure region, this approach for the practical injection condition has limitations for simulation of realistic injections. Because the CO_2 density changes with the temperature and pressure condition, the CO_2 density at the injection point varies with the selected reservoir condition. Moreover, the CO_2 density also increases with the pressurization at the injection well caused by the CO_2 injection. The injection pressure is decreased at the lower reservoir temperature and higher hydrostatic pressure condition. The lower is reservoir temperature, the lower is the injection pressure because the CO_2 volume flow rate is decreased with increasing CO_2 density. These results indicate that it is attractive to select a CO_2 injection site whose condition preserves the CO_2 density high for the sake of preventing excessive pressurization around the injection well. The CO_2 permeation is also strongly affected by the CO_2 state in the reservoir. The CO_2 saturation becomes higher with increasing reservoir temperature. The analysis for the distribution of the spatial CO_2 saturation is directly connected to the capacity estimation for the reservoir for CO_2 geological sequestration. Additionally, selecting the injection site that has low temperature and higher hydrostatic pressure may allow long term injection because it may prevent the increase of pressure in the reservoir and CO_2 permeation to a distance. At the same time, the capacity of the reservoir may become larger under the lower temperature and hydrostatic pressure condition. Consequently, these results indicate that the reservoir condition is a key factor to determine the project details of CO_2 geological sequestration.

References

[1] Metz B, Davidson O, de Coninck H, Loos M, Meyer L, editors. IPCC, 2005: IPCC Special report on carbon dioxide capture and storage. Prepared by Working Group of the Intergovernmental Panel on Climate Change, Cambridge University press, Cambridge, 2005.

[2] IEA Greenhouse Gas R&D Programme, Putting carbon back into the ground. Online Report, 2001, Available from: www.ieagreen.org.uk/ccs.html.

[3] Xu T, Apps JA, Pruess K. Reactive geochemical transport simulation to study mineral trapping for CO_2 disposal in deep arenaceous formations. J Geophys Res 2003;108(B2):3-1–3-13.

[4] Bachu S. Sequestration of CO_2 in geological media: criteria and approach for site selection in response to climate change. Energy Convers Manage 2000;41:953–70.

[5] Bachu S, Adams JJ. Sequestration of CO_2 in geological media in response to climate change: capacity of deep saline aquifers to sequester CO_2 in solution. Energy Convers Manage 2003;44:3151–75.

[6] Hitchon B. Aquifer disposal of carbon dioxide hydrodynamic and mineral trapping – proof of concept. Sherwood Park Alberta, Canada: Geoscience Publishing Ltd; 1996.

[7] Class H, Helmig R, Bastian P. Numerical simulation of non-isothermal multiphase multicomponent processses in porous media. 1. an efficient solution technique. Adv Water Resour 2002;25:533–50.

[8] Chadwick RA, Zweigel P, Gregersen U, Kirby GA, Holloway S, Johannessen PN. Geological reservoir characterization of a CO_2 storage site: the Utsira Sand, Sleipner, Northern North Sea. Energy 2004;29:1371–81.

[9] Pruess K. TOUGH2 – A general purpose numerical simulator for multiphase fluid and heat flow. Univ Calif: Lawrence Barkeley Laboratory; 1991.

[10] Talman SJ, Adams JJ, Chalaturnyk RJ. Adapting TOUGH2 for general equations of state with application to geological storage of CO_2. Comput Geosci 2004;30:543–52.

[11] Span R, Wagner W. A new equation of state for carbon dioxide covering the fluid region from the triple-point temperature to 1100 K at pressures up to 800 MPa. J Phys Chem Ref Data 1996;25:1509–96.

[12] Law DHS, Bachu S. Hydrogeological and numerical analysis of CO_2 disposal in deep aquifers in the Alberta sedimentary basin. Energy Convers Manage 1996;37:1167–74.

[13] Bachu S. Sequestration of CO_2 in geological media in response to climate change: road map for site selection using the transform of the geological space into the CO_2 phase space. Energy Convers Manage 2002;43:87–102.

[14] Gaus I, Azaroual M, Czernichowski-Lauriol I. Reactive transport modelling of the impact of CO_2 injection on the clayey cap rock at Sleipner (North Sea). Chem Geol 2005;217:319–37.

[15] Torp TA, Gale J. Demonstrating storage of CO_2 in geological reservoirs: the Sleipner and SACS projects. Energy 2004;29:1361–9.

[16] Root RS, Gibson-Poole CM, Lang SC, Streit JE, Underschultz J, Ennis-King J. Opportunities for geological storage of carbon dioxide in the offshore Gippsland Basin, SE Australia: an example from the upper Latrobe Group. In: PESA Eastern Australasian Basins Symposium 2004; p.367–388.

[17] Cook PJ, Rigg A, Bradshaw J. Putting it back where it came from: is geological disposal of carbon dioxide an option for Australia? APPEA J 2000;40(1):654–66.

[18] NEDO/RITE. Research and development of underground storage technology for carbon dioxide, 2002 [in Japanese].

[19] Helmig R. Multiphase flow and transport processes in the subsurface – a contribution to the modeling of hydrosystems. Heidelberg: Springer; 1997.

[20] Fagerlund FF, Niemi A, Odéen M. Comparison of relative permeability-fluid saturation-capillary pressure relations in the modelling of non-aqueous phase liquid infiltration in variably saturated, layered media. Adv Water Resour 2006;29:1705–30.

[21] Span R, Wagner W, Lemmon EW, Jacobsen RT. Multiparameter equations of state – recent trends and future challenges. Fluid Phase Equilibria 2001;183–184:1–20.

[22] Sasaki K, Fujii T, Hashida T. Numerical simulation of flow dynamics for CO_2 injection into rock masses. AIP Conf Proc 2006;832:433–8.

[23] Ferziger JH, Perić M. Computational methods for fluid dynamics. Tokyo: Springer Verlag Tokyo; 2003.